ROUGHNESS EFFECTS ON SUB-PIXEL RADIANT TEMPERATURES IN KINETICALLY ISOTHERMAL SURFACES

Iryna Danilina[1], Amit Mushkin[1], Alan Gillespie[1], Michael O'Neal[2], Lisa Pietro[2], Lee Balick[3]

1 Department of Earth and Space Sciences, University of Washington, Seattle WA 98195-1310 USA;
2 Department of Geography, University of Delaware, Newark DE 19716 USA;
3 Space & Remote Sensing Sciences Group (ISR-2), Los Alamos National Laboratory M/S B244, P.O. Box 1663, Los Alamos, NM 87545 USA

Communicating author: danilina@u.washington.edu

ABSTRACT - *Temperature/emissivity estimation from remotely measured radiances generally assumes that scene elements represented by pixels in fact have a single emissivity spectrum and are isothermal. Thus, estimated temperatures and emissivities are effective values that would be found if these simplified assumptions were met. In reality, the physical scene is neither homogeneous nor isothermal, and the effective values are not strictly representative of the scene. How much in error are they? In this study we report on the dispersion of radiant temperature from the unresolved scene elements comprising a pixel due to roughness for the simple case when the scene actually is isothermal: i.e., the kinetic (but not radiant) temperature is everywhere the same. We use a radiosity model adapted for thermal infrared and driven by cm-scale digital terrain models (DTMs) measured by LiDAR. The DTMs cover small (0.5-10 m) areas of natural surfaces in the Mojave Desert, California (USA). Also we use high-resolution FLIR images of the same natural surfaces to test the model predictions for the homogeneous scenes. The differences between effective and kinetic temperatures and the variance of the calculated radiant temperature distributions are reported as functions of root-mean-squared (RMS) elevations within the modeled terrain.*

1 INTRODUCTION

In thermal-infrared (TIR) imaging it is necessary to integrate the radiant flux from the scene over the pixel projected on the ground, and then use one of several algorithms (*e.g.,* *Gillespie et al*., 1998; *Wan & Li,* 1997; *Sobrino & Li*, 2002, *Jimenez-Munoz et al*., 2006) to estimate effective temperatures and emissivities for the surface. Provided the surface is smooth, homogeneous, and isothermal, the values of the effective parameters are within a degree or two, or within ~0.015 emissivity units, of the values measured *in situ* (*e.g., Gillespie et al.,* 1998). What happens if these fundamental assumptions are violated? The answers will become more important as technology improvements allow imaging with higher spatial and radiometric resolution.

Some studies have addressed simplified versions of the general problem. *Dozier* (1981) estimated snow cover assuming that the pixel represented a binary mixture of snow-covered and bare components; *Pieri et al.* (1990) applied similar reasoning to determine temperatures for unresolved lava effusions viewed against a background of cooled lava; and *Gustafson et al*. (2002) considered extraction of temperatures of unresolved stream elements. All these studies used the simplifying assumption that the scene consisted of two unresolved components, each homogeneous. *Gillespie* (1992) considered the more general case in which the scene contained multiple spectral endmembers, but nevertheless assumed each pixel was isothermal.

We have investigated the dispersion of temperatures and emissivities that occur as the assumed conditions – that scene elements are isothermal, smooth, and homogeneous – are relaxed. In this paper we report on the findings relevant to temperature, from analysis of TIR images and digital terrain models (DTMs) at the 1-10 cm scale, the scale at which the basic building blocks, such as gravel and jointed bedrock, of the landscape are resolved. We restrict discussion to unvegetated surfaces.

2 APPROACH

Natural scenes used in our experiment were monolithologic expanses of bedrock and alluvial surfaces in the Mojave Desert, California (Fig. 1). We studied 0.5-m to 10-m landscapes from four

geographic sites. The Kit Fox site is from the alluvial fans below the Kit Fox Hills, on the east side of Death Valley. The Mars Hill site is near Artist's Drive, on the east side of Death Valley. The Dogleg site is a 90º kink in a fluvial channel on Trail Canyon Fan on the west side of Death Valley. The Alabama Hills site is from the pediment near Movie Flats, west of the Alabama Hills in Owens Valley.

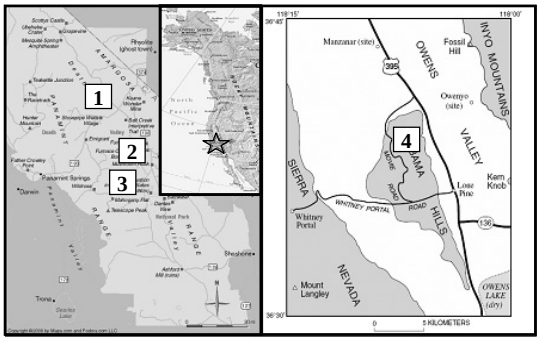

Figure 1. *Map showing locations of field test sites. Death Valley (left): 1 – Kit Fox site; 2 – Mars Hill site; 3 – Dogleg site. Owens Valley (Right): 4 – Alabama Hills site.*

We generated high-resolution DTMs from tripod-mounted LiDAR (Trimble GS-2000) measurements. We developed the radiosity model (form-factor approach) for predicting temperature effects due to scene roughness. Radiant temperature images were measured at various view angles using a FLIR broadband TIR camera (FLIR Systems Inc.) with NE□T≈0.3 K. Images made before sunup were the most closely isothermal, and were used for testing the developed model predictions. Examples of a DTM used is given in Figure 2.

2.1 Radiosity model

The total radiance from the surface element, consisting of energy emitted by this surface element and the reflected energy of adjacent surface elements, is called radiosity, and models that predict it are called radiosity models. Radiosity models for visible and near- and shortwave-infrared wavelengths include reflected direct sunlight (*Li*, 1997), but this term is negligible in the TIR.

We consider the simplistic case of thermal radiance from a homogeneous isothermal surface. This condition arguably approximates a surface at dawn, but is not appropriate for surfaces being heated by the sun. We assumed all surfaces were Lambertian, that is they were perfect diffusers and emitted and reflected radiation isotropically, according to Lambert's law. As the study evolves, we intend to include a heating term and anisothermal surfaces in the TIR radiosity model.

1)

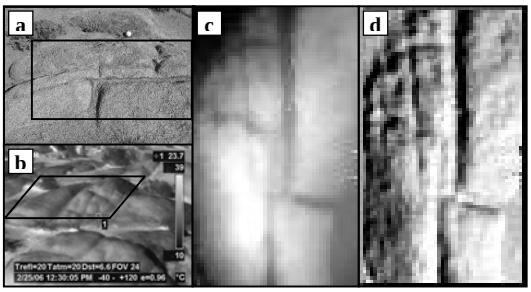

2)

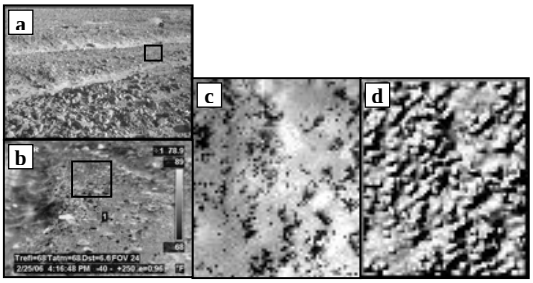

Figure 2. *Examples of data used. 1): Natural bedrock surface (Alabama Hills site), surface size is 1.4 m by 2.5 m. a – photo of the surface; b – FLIR image of the surface; c - DTM (resolution is 3 cm, number of pixels is 4042); d – shaded relief image. 2): Alluvial fan surface (Kit Fox site), surface size is 0.6 m by 0.75 m. a – photo of the surface; b – FLIR image of the surface; c - DTM (resolution is 1 cm; number of pixels is 4636); d – shaded relief image.*

The general form of a radiosity model in our case is written as:

$$B_i = R_i + MS_i, \qquad i = 1,2\ldots n, \tag{1}$$

where B_i – radiosity of a surface element;

R_i – thermal energy released from a surface element;

MS_i – multiple scattering component (energy bounced one or more times among surface elements);

n – number of surface elements.

The radiation emitted by a blackbody surface at any given wavelength is described by Planck's Law. But natural surfaces usually do not behave as perfect emitters, so Planck's function must be modified by including emissivity ε. Emissivity is defined as the ratio between the measured surface-emitted radiation and the radiation expected from a blackbody at the same kinetic temperature. In this study, we are

interested in wavelength range from 8 μm to 14 μm (thermal part of spectrum). We assume our surfaces to be a greybody in this interval: *i.e.,* ε is independent of wavelength. Thus, surface radiance is given by

$$R = \varepsilon \cdot \int_{\lambda_1}^{\lambda_2} \frac{c_1}{\lambda^5} \cdot \frac{1}{e^{c_2/\lambda T} - 1} \cdot d\lambda \,, \qquad (2)$$

where R – thermal energy released from a surface;

ε – emissivity of a surface;

$c_1 = 3.74 \cdot 10^{-16} W \cdot m^2$ – first radiation constant;

$c_2 = 0.0144\ m \cdot K$ – second radiation constant;

$\lambda_1 = 8 \cdot 10^{-6}\ m$ – lower limit of the thermal part of the spectrum;

$\lambda_2 = 14 \cdot 10^{-6}\ m$ – upper limit of the thermal part of the spectrum;

T – kinetic temperature of a surface.

The main complication of the radiosity model is calculation of the multiple-scattering component. The amount of energy reflected from adjacent surface elements is determined by their geometric relation, which can be established using DTMs, slope, and aspect information. This geometric relation is called the "form factor" and is defined as fraction of energy leaving one surface element and reaching another.

The full radiosity model is written as:

$$B_i = R_i + \rho \cdot \sum_{j=1}^{n} B_j \cdot F_{ij}\,, \quad i, j = 1, 2 \ldots n\,, \qquad (3)$$

where ρ – reflectivity of a surface;

F_{ij} – form factor from surface element j to surface element i.

here are n unknown radiosities and n linear equations associated with individual pixels. Rearranging equation (3), the n linear equations can written in a matrix expression:

$$\begin{bmatrix} 1-\rho F_{11} & \ldots & -\rho F_{1n} \\ -\rho F_{21} & \ldots & -\rho F_{2n} \\ \vdots & & \vdots \\ -\rho F_{n1} & \ldots & 1-\rho F_{nn} \end{bmatrix} \cdot \begin{bmatrix} B_1 \\ B_2 \\ \vdots \\ B_n \end{bmatrix} = \begin{bmatrix} R_1 \\ R_2 \\ \vdots \\ R_n \end{bmatrix}. \qquad (4)$$

For the isothermal surfaces with an assumed temperature, R is a known constant calculated using Planck's Law. The key step of the radiosity model is determining form factor matrix F. The basic form of form factor describes the radiance emitted from one point and incident on another (*Sparrow*, 1963, *Sparrow & Cess*, 1978):

$$F_{dE_j - dE_i} = \frac{\cos\theta_i \cdot \cos\theta_j}{d^2 \cdot \pi} \cdot dA_i \qquad (5)$$

where $F_{dE_j - dE_i}$ – form factor from surface element; dE_j to surface element dE_i;

θ – projection angle between the normal of a surface element and line, linking the pair of elements together;

dA_i – area of element dE_j;

d – the distance between two elements.

Using equation (5), the form-factor matrix F (eqn. 3 -5) can be constructed. Terms from equation (5) are illustrated in Figure 3.

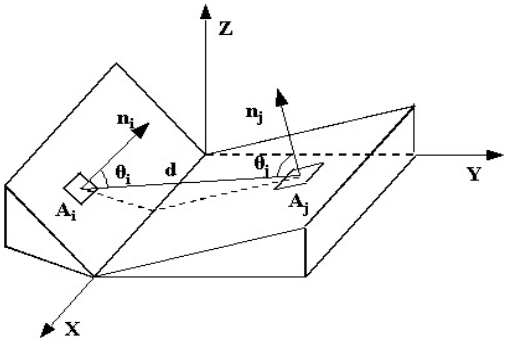

Figure 3. *Schematic plot illustrating terms used in form-factor equation.*

3 RESULTS AND DISCUSSION

The TIR radiosity model was run for fourteen DTMs: ten alluvial surfaces from the "Dogleg" and "Kit Fox" sites; two bedrock expanses from the Alabama Hills site (model results for one of Alabama Hills DTMs and Kit Fox site DTM are shown in Fig. 4), and two surfaces from the "Mars Hill" site (Fig. 1).

To test the model we used predawn FLIR image of one of the surfaces at Alabama Hills site. Radiant temperature distribution predicted by the model was quite similar to measured by the FLIR camera. However, radiosity values were slightly underestimated by the model (i.e. maximum kinetic temperature in the scene predicted by the model is about 1 degree lower than maximum measured temperature). It can be explaned by the fact that the simple formulation of form factor used in our model tends to underestimate fraction of scattered energy. Energy scattered to the observed scene from larger-

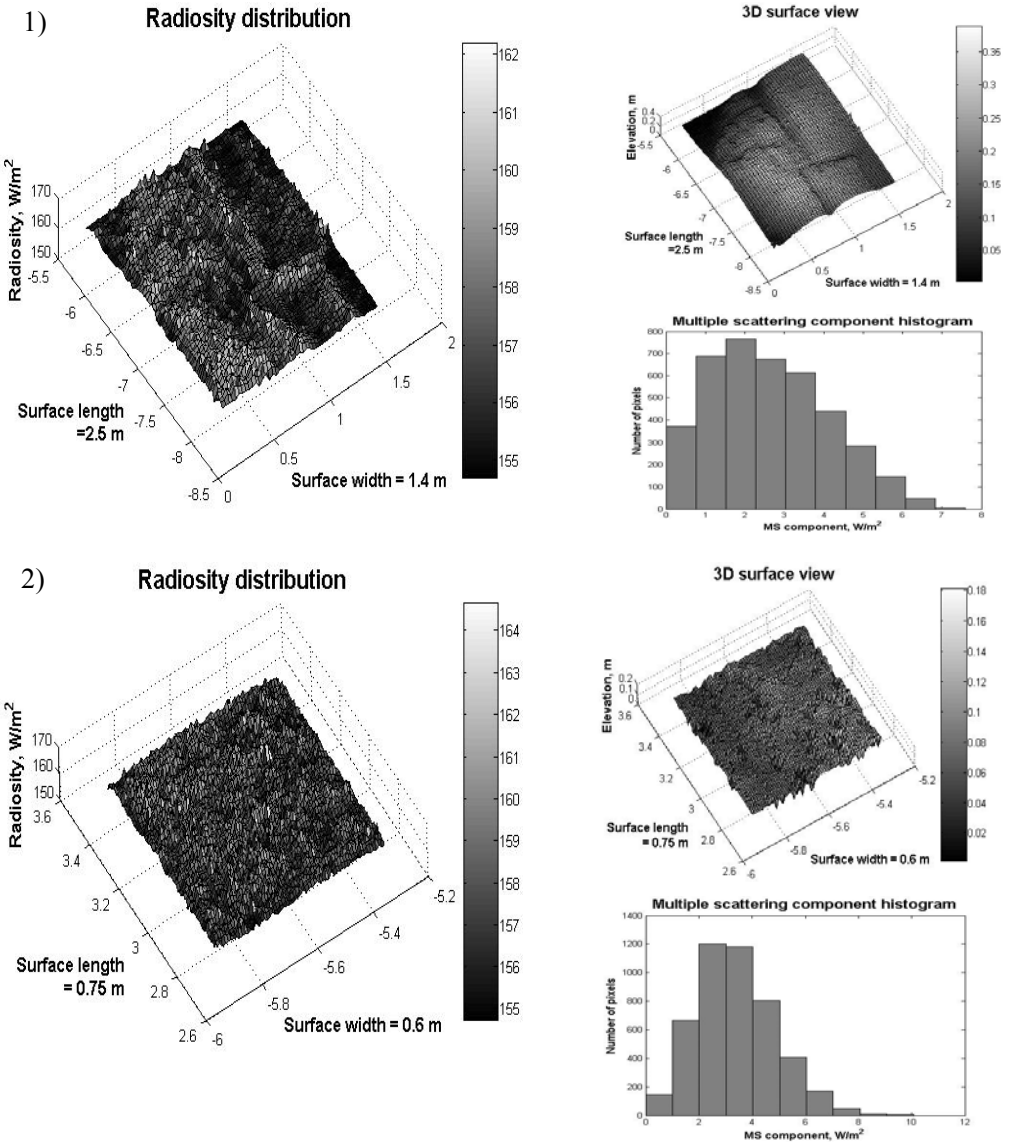

Figure 4. *Examples of radiosity model results. 1) Radiosity distribution, 3D surface view and multiple scattering component diagram for one of the Alabama Hills site (see Fig. 2). Kinetic temperature = 300 K; surface emissivity = 0.9; surface RMS = 0.084 m; mean radiosity = 157.29 W m^{-2}; radiosity RMS = 1.48 W m^{-2}; predicted effective temperature minus prescribed kinetic temperature : ΔT = 1.12 K; predicted emissivity minus prescribed emissivity: $\Delta\varepsilon$= 0.015. 2) Radiosity distribution, 3D surface view and multiple scattering component diagram for the Kit Fox site (see Fig. 2). Kinetic temperature = 300 K; surface emissivity = 0.9; surface RMS = 0.027 m; mean radiosity = 158.03 W m^{-2}; radiosity RMS = 1.49 W m^{-2}; predicted effective temperature minus prescribed kinetic temperature : ΔT = 1.44 K; predicted emissivity minus prescribed emissivity: $\Delta\varepsilon$= 0.02.*

scale surrounding objects (e.g., Sierra Nevada mountains) was not taken into account, which can also cause lower predicted radiant temperatures.

The radiosity model predicted surface RMS roughness values ranging from 0.016 to 0.174 m, RMS radiosity values ranging from 1.21 to 2.04 W m^{-2}, and mean radiosity values ranging from 156.7 to 158.85 W m^{-2}. The difference between effective and kinetic temperature values ranged from 0.61 to 1.78 K, and the difference between effective and prescribed emissivity values ranged from 0.012 to 0.024.

The radiosity model results also showed that, for the isothermal alluvial surfaces, the radiosity dispersion and the difference between kinetic and effective temperatures increase with surface roughness (Fig. 5). These findings confirm the expectations that led us to these experiments: that is, cavity and multiple-scattering effects – departures from the ideal Lambertian surface – lead to disparity between recovered effective temperatures and the actual kinetic temperatures of surfaces.

Results for other types of surfaces, for example the bedrock surfaces of the Alabama Hills, do not plot on the same trend lines. One possible explanation for this is the fact that, in alluvial surfaces, roughness is evenly distributed and radiosity dispersion depends only on the scale of roughness. For other types of surfaces, including the bedrock examples, this is not the case. Surface organization for such surfaces is complex and hard to predict statistically. Perhaps after analyzing more examples some relationship can be established. However, the difference in behavior between alluvial and bedrock surfaces itself is a useful finding, identifying a potential stumbling block should statistical surface roughness estimates be used to correct for temperature and emissivity dispersion in future efforts and algorithms.

5 CONCLUSIONS

Radiant temperatures from complex surfaces vary because of reflection of heat from adjacent scene elements, added to the energy radiated in proportion to the kinetic temperature. The distribution of radiant temperature depends on the roughness and surface organization and is difficult to predict with simple statistical models that do not take into consideration the organization of surface roughness elements. The effective emissivity also varies because reflection and emission are complementary (cavity effect), and thus for very rough surfaces the emissivity approaches unity.

We have assumed for modeling that the kinetic temperature is everywhere the same, but this ideal condition is rarely realized in the field because some scene elements shadow others, because radiation of energy cools surfaces preferentially, established near-surface thermal gradients, and because of absorption of heat radiated from nearby slopes. It can be seen from our radiosity model that, even given our simplifying assumptions that minimize the effect, the disparity between effective temperatures from real ones is on the order of a few degrees, big enough to affect some important TIR remote-sensing applications, such as for energy-balance studies. For anisothermal surfaces, temperature dispersion is likely to increase with solar heating of exposed surface elements. It also follows that apparent emissivity will change over the course of the day, as cavities change from cooler to warmer than interstices.

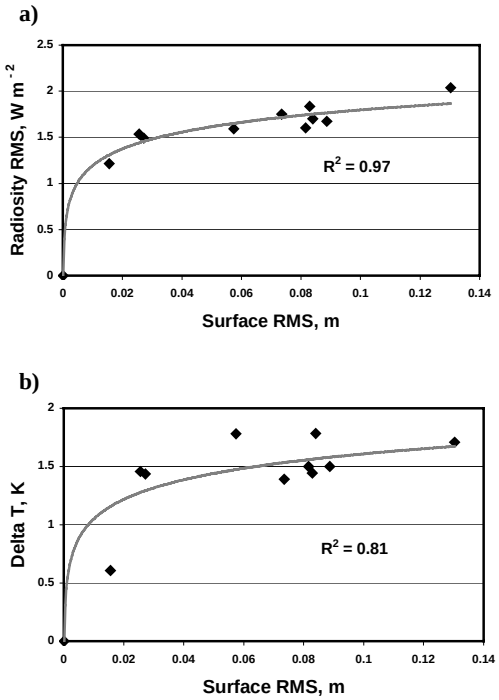

Figure 5. *Effect of surface RMS on radiosity dispersion in alluvial scenes. a) Radiosity RMS vs. surface roughness. The r^2 value for the regression is 0.97.*
b) Prescribed kinetic temperature minus predicted effective temperatures (Delta T) vs. surface roughness. The r^2 value for the regression is 0.81.

We anticipate that, in the near future, dispersion of radiometric temperatures within a pixel will be measured over the course of a day, as sun-facing surfaces or surfaces with low thermal inertias are heated relative to their shadowed or high-inertia counterparts. Modeling based on these data should give a more realistic, quantitative estimate of the errors in recovered temperatures and emissivities due to surface roughness.

AKNOWLEDGEMENTS

Research supported by subcontract PR32449 from Los Alamos National Laboratory.

REFERENCES

Dozier, J., 1981. A method for satellite identification of surface temperature fields of subpixel resolution. Remote Sensing of Environment 11, 221-229, doi:10.1016/0034-4257(81)90021-3.

Gillespie, A. R., 1987. Lithologic mapping of silicate rocks using TIMS data. *Proceedings of the Workshop on Thermal Infrared Multispectral Scanner*, Jet Propulsion Laboratory Publication 36-38, Pasadena, CA, 29-44.

Gillespie, A. R., 1992. Spectral mixture analysis of multispectral thermal infrared images. *Remote Sensing of Environment* 42, 137-145.

Gillespie, A. R., Cothern, J. S., Matsunaga, T., Rokugawa, S., and Hook, S. J., 1998. Temperature and Emissivity Separation from Advanced Spaceborne Thermal Emission and Reflection Radiometer (ASTER) Images. *Institute of Electrical and Electronics Engineers (IEEE) Transactions on Geoscience and Remote Sensing* 36, 1113-1126.

Gustafson, W. T., Handcock, R. N., Gillespie, A. R., and Tonooka, H., 2002. An image-sharpening method to recover stream temperatures from ASTER Images. *International Society for Optical Engineering (SPIE) Workshop: Remote Sensing for Environmental Monitoring, GIS Applications, and Geology II*, Crete, Greece, Sept. 23-27.

Jimenez-Munoz, J. C, Sobrino, J. A., Gillespie, A., Sabol, D., Gustafson, W. T, 2006. Improved land surface emissivities over agricultural areas using ASTER NDVI. *Remote Sensing of Environment* 103, 474-487.

Li, W. -H., 1997. Significance of multiple scattering in remotely sensed images of natural surfaces. PhD dissertation., University of Washington, Seattle.

Pieri, D. S., Glaze, L. S., Abrams M. J., 1990. Thermal radiance observations of an active *lava* flow during the June 1984 eruption of Mount Etna. *Geology* 18, no.10, 1018-1022.

Sobrino, J. A., Li, Z. –L, 2002. Land surface temperature and emissivity retrieval from remote sensing data. *Recent Research Developments in Geophysics* 4, 21-44.

Sparrow, E., 1963. A new and simple formulation for radiative angle factors. *American Society of Mechanical Engineers (ASME) Journal of Heat Transfer* 85, 81-88.

Sparrow, E., and Cess, R., 1978. *Radiation heat transfer*. Hemisphere Publishing, Washington D.C., 366 pp.

Wan, Z., Li, Z. -L., 1997. A physics-based algorithm of retrieving land-surface emissivity and temperature from EOS/MODIS data. *Institute of Electrical and Electronics Engineers (IEEE) Transactions on Geoscience and Remote Sensing* 36, 980-996.